Performance Prediction of Single-Sided Induction Heating System

J. H. H. Alwash, *Member, IEEE*, and S. K. Sultan

***Abstract*—Surface induction heating is nowadays widely used with coil arrangement varied according to the work piece topology. For a flat work piece arrangement, the coil may be of the single-conductor type or single-coil type, and finally, it may be of multicoil type. It is thought that the development of a generalized approach to analyze all three possible excitation systems mentioned earlier is an important task. In this paper, a generalized approach using a multilayer electromagnetic model is presented to analyze all three possible excitation arrangements. The theoretical results are compared with the experimental findings and with theoretical results obtained using other approaches.**

***Index Terms*—Hardening, induction heating, surface heating.**

List of Principal Symbols

B	Flux density (in tesla).
B_z	Peak value of resultant z-direction flux density.
E	Electric field strength (in volts per meter).
E_x	Peak value of resultant x-direction electric field strength.
F	Frequency (in hertz).
H	Magnetic field strength (in ampere per meter).
H_y	Peak value of resultant y-direction magnetic field strength.
I	Exciting current (in ampere).
J	Line current density (in ampere per meter).
J_S	Slot current density (in ampere per meter) $= (N_t I)/S_L$.
n	Harmonic number.
N_t	Turns per coil.
ρ	Resistivity (in ohm meter).
P_L	Pole width (in meter).
S	Power density (in watt per square meter).
S_L	Slot width (in meter).
W	Half period of current density wave.
ω	$2\pi fI$.
σ	Conductivity (in mho per meter).
μ_0	Permeability of free space (in henry per meter).
μ_m	Relative permeability of region (in meter).

I. Introduction

SURFACE induction heating can be achieved by different types of induction heating systems depending on the work piece geometry. For a flat specimen, single-sided induction heating system may be used [1]–[8].

The exciting winding, in its two types, air cored or iron cored, can be formed as a single coil system [2], [3] or as a single conductor [6], or as a multicoil system [4].

The object of this paper is to present a generalized analytical method using the multilayer approach [9] to investigate the performance of surface induction heating system for flat work piece, with all possible versions of excitation, i.e., single coil, multicoil, or single conductor. To validate the theoretical analysis, the results obtained are compared with the experimental findings and with theoretical results obtained using other approaches.

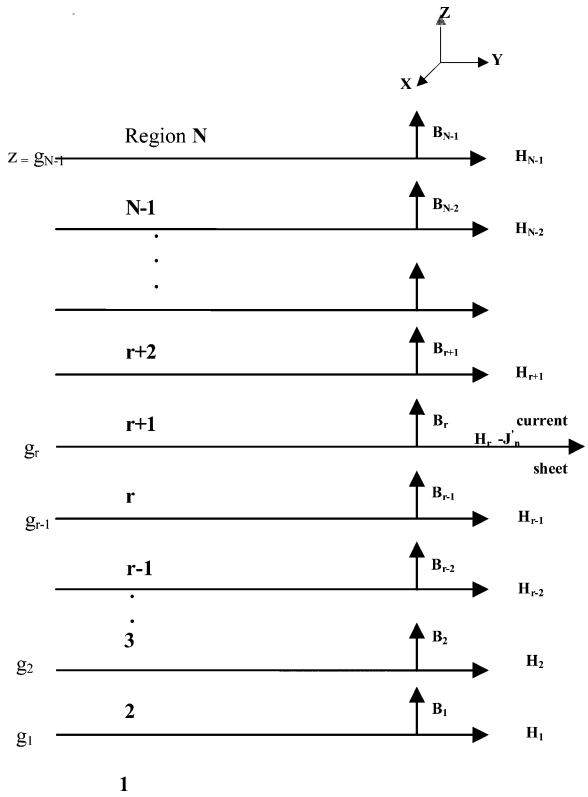

Fig. 1. General multiregion model.

II. Mathematical Model

The mathematical model chosen for analysis is a general multilayer problem, and it is clear that each region (Fig. 1) is characterized by its permeability and conductivity. It should be appreciated that the main assumptions in this case may be summarized as follows:

Manuscript received May 8, 2004; revised August 7, 2008 and March 5, 2009; accepted January 7, 2010. Date of publication November 8, 2010; date of current version November 19, 2010. Paper no. TEC-00136-2004.

The authors are with the Electrical Engineering Department, College of Engineering, University of Baghdad, 47019 Baghdad, Iraq (e-mail: jalwash@hotmail.com).

Digital Object Identifier 10.1109/TEC.2010.2041666

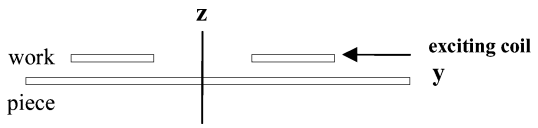

Fig. 2. General single-coil system.

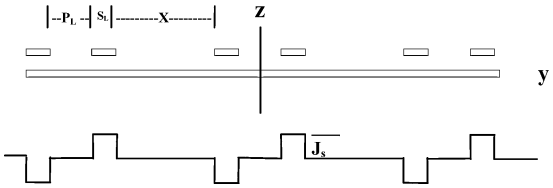

Fig. 3. General series of single coils and the corresponding line current density wave.

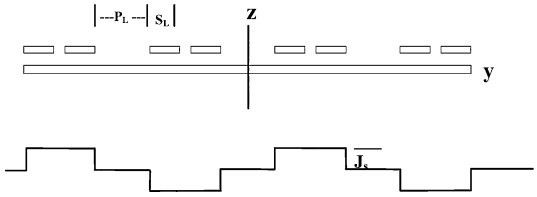

Fig. 4. Multicoils system and its line current density waveform.

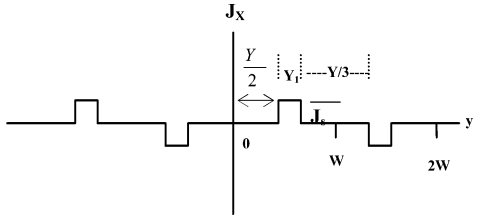

Fig. 5. General line current density waveform.

1) Each region is of infinite extent in the *x–y* plane, thus all end effects are considered negligible.
2) Saturation effects are ignored.
3) The displacement currents are considered negligible.
4) All field components disappear at $\mathbf{z} = \pm\infty$.
5) The current sheet is of infinite extent in the **x**-direction and infinitely thin in **z**-direction, and lies between region *r* and region $r+1$.
6) Normal component of magnetic flux density B_z is continuous across a boundary, and the tangential component of magnetic field strength H_y is continuous across a boundary except at the current sheet where a discontinuity equal to the line current density exists where:
   H_r = Magnetic field strength below current sheet.
   $H_r - \mathrm{J}'_n$ = Magnetic field strength above current sheet.

The exciting coils are usually fed in most cases from single-phase supply, where the resulting multimode fiber is of the pulsating type. However, it is well known that such a field may easily be resolved into two components—forward and backward traveling fields. It is, therefore, justified to analyze the general model for the case where only pure traveling field exists. The final results may be obtained through superposition.

III. Current Sheet Representation

Since the exciting winding of the heating system is considered to be fed from single-phase power supply, then the model is subjected to a pulsating field which can be resolved into two counter revolving fields. Fig. 2 shows a general single-coil system of excitation. To facilitate Fourier analysis, it is assumed that the system of excitation is made up of a series of such coils, as shown in Fig. 3, which also shows the corresponding line current density curve. *x* is assumed large enough and approaches infinity.

Fig. 4 shows a multicoil arrangement and its corresponding line current density wave.

To generalize the waveform analysis, Fig. 5 shows a general waveform which may be taken to represent both the single coil and multicoil system as follows:

1) For multicoil system $Y_1 = 2S_L \,\&\, Y_2 = Y_3 = P_L$.
2) For single-coil system $Y_1 = S_L \,\&\, Y_2 = P_L \,\&\, Y_3 \to \infty$.

It can easily be seen that the waveform may further be considered to represent a single-conductor system with
$Y_1 = S_L \,\&\, Y_2 = Y_3$ and both approach infinity.

Using Fourier analysis to the general waveform represented by Fig. 5, where the wave has an odd symmetry (i.e., $F(y) = -F(-y)$), then the current sheet may be written

$$J_x = \sum_{n=1}^{\infty} 2J'_n \sin(\omega t)\sin\left(\frac{n\pi}{W}y\right) \tag{1}$$

where

$$J'_n = \frac{N_t I}{n\pi Y_1}\left[\cos\left(\frac{n\pi Y_2}{2W}\right) - \cos(n\pi)\cos\left(\frac{n\pi Y_a}{2W}\right)\right]$$

or

$$J_x = \sum_{n=1}^{\infty} J'_n\left(\left(\cos\left(\omega t - \frac{n\pi}{W}y\right) - \cos\left(\omega t + \frac{n\pi}{W}y\right)\right)\right.$$

This form of the line current density can be resolved into two counter revolving components

$$J_x = J_n - J_{nb}$$

where

$$J_n = \sum_{n=1}^{\infty} J'_n \mathrm{Re}(e^{j(\omega t - k_n y)}) \tag{2}$$

$$J_{nb} = \sum_{n=1}^{\infty} J'_n \mathrm{Re}(e^{j(\omega t + k_n y)}). \tag{3}$$

IV. Mathematical Analysis

Now Maxwell equations for general region may be written as

$$\mathrm{curl}\, H = J$$

$$\mathrm{curl}\, E = \frac{-\partial B}{\partial t}$$

$$\mathrm{div} B = 0$$

$$\mathrm{div} J = 0$$

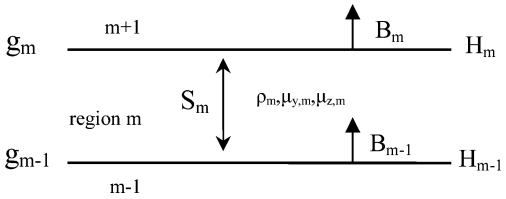

Fig. 6. General region *m*.

and

$$B = \mu_0\, \mu_m\, H$$

$$E = \rho J.$$

The forward field in a region varies everywhere as $\mathrm{Re}(\exp(j(\omega t - k_n y)))$. Hence, the solution of the Maxwell equations for a general region *m*, shown in Fig. 6, may be presented as follows:

$$\frac{\partial^2 Bz}{\partial z^2} = \gamma_m^2\, Bz$$

where

$$\gamma_m = \left(k_n^2 + \frac{j\omega\mu_o\mu_m}{\rho}\right)^{\frac{1}{2}}$$

and the solution of this second-order differential equation is

$$Bz = A\cosh(\gamma_m z) + C\sinh(\gamma_m z) \tag{5}$$

where *A* and *C* are constants to be found from the boundary conditions.

Then, from div $B = 0$

$$Hy = \beta_m\,(A\sinh(\gamma_m z) + C\cosh(\gamma_m z)) \tag{6}$$

where

$$\beta_m = \frac{\gamma_m}{jk_n\mu_y\mu_o}$$

and from curl $E = \dfrac{-\partial B}{\partial t}$

$$E_x = \frac{-\omega}{k_n} B_z. \tag{7}$$

Fig. 6 shows a general region *m* of thickness S_m. The normal component of flux density on the lower boundary is B_{m-1}, and the tangential component of magnetic field strength is H_{m-1}. The corresponding values on the upper boundary are B_m and H_m.

To predict a relation between the upper boundary and the lower boundary field component, (5) and (6) can be solved at the lower boundary of region *m*, where $Z = g_{m-1}$, and at the upper boundary, where $Z = g_{m-1} + S_m$. Then, we get

$$\begin{bmatrix} B_m \\ H_m \end{bmatrix} = \begin{bmatrix} \cosh(\gamma_m S_m) & \dfrac{1}{\beta_m}\sinh(\gamma_m S_m) \\ \beta_m \sinh(\gamma_m S_m) & \cosh(\gamma_m S_m) \end{bmatrix} \begin{bmatrix} B_{m-1} \\ H_{m-1} \end{bmatrix} \tag{8}$$

or

$$\begin{bmatrix} B_m \\ H_m \end{bmatrix} = [T_m] \begin{bmatrix} B_{m-1} \\ H_{m-1} \end{bmatrix} \tag{9}$$

where

$$[T_m] = \text{Transfer matrix of region}\, m.$$

Solving the field in the bottom region, we get

$$H_1 = \beta_1 B_1 \tag{10}$$

and also solving the field in the top region, we get

$$H_{N-1} = -\beta_N B_{N-1}. \tag{11}$$

Now with reference to Fig. 1 and assumption (6), the field in regions *N* to $r + 1$ situated above the current sheet may be presented through the use of (8) which may be rewritten in the following manner:

$$\begin{bmatrix} B_{N-1} \\ H_{N-1} \end{bmatrix} = [T_{N-1}]\,[T_{N-2}]\cdots[T_{r+1}] \begin{bmatrix} B_r \\ H_r - J_n' \end{bmatrix} \tag{12}$$

$$\begin{bmatrix} B_r \\ H_r \end{bmatrix} = [T_r]\,[T_{r-1}]\ldots[T_2] \begin{bmatrix} B_1 \\ H_1 \end{bmatrix}. \tag{13}$$

These two sets of equations can be solved for the flux density B_1 by making use of (10) and (11). Then, the tangential component H_1 can be calculated using (10). All boundary values below the current sheet may then be calculated using (13). Finally, using (12), the values of the other regions' boundaries above the current sheet can be calculated.

Now, the values of B_z, H_y, and E_x due to the forward component of the current sheet may be evaluated. The corresponding resultant values can then be calculated through the superposition as

$$B = \hat{B}_z \cos\left(\frac{n\pi}{W} y\right) \tag{14}$$

$$H = \hat{H}_y \sin\left(\frac{n\pi}{W} y\right) \tag{15}$$

$$E = \hat{E}_x \sin\left(\frac{n\pi}{W} y\right). \tag{16}$$

The power density at any point can be calculated as the cross product of the electric field and magnetic field strength and may be represented as

$$S = \hat{E}_x \hat{H}_y \left(\sin\left(\frac{n\pi}{W} y\right)\right)^2. \tag{17}$$

V. Results

Three models are chosen to evaluate the theoretical analysis. These include the single-coil, single-conductor, and multicoil excitation systems.

A. Single-Coil Excitation System

The model in this case is that presented by [3]. The data are tabulated in Table I and Fig. 7(a) shows the general model layout.

Now the multilayer mathematical model may easily be constructed as shown in Fig. 7(b).

Figs. 8 and 9 show the theoretical results obtained using the numerical method presented by Patecki and Szymanski [3] and that obtained using the multilayer approach presented in this paper.

It can be seen that the two sets of results correlate well.

TABLE I
SINGLE-COIL MODEL DATA

Parameter	Value
Slot width S_L	0.001 m
Pole width P_L	0.04 m
Coil width 2w	0.25 m
Conductivity of conducting plate	$1x10^6$ moh.m^{-1}
Relative permeability of conducting plate	30
Non magnetic ferromagnetic bar dimension	0.06 m x 0.03 m
Its relative permeability	700
Exiting current	1A
Frequency range	1 KHz & 2.4 KHz

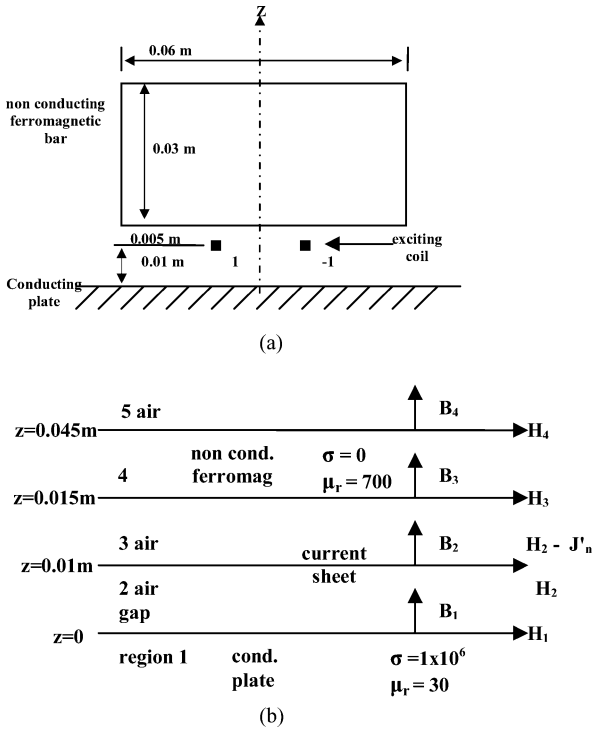

Fig. 7. Single-coil model: (a) model layout, (b) mathematical model.

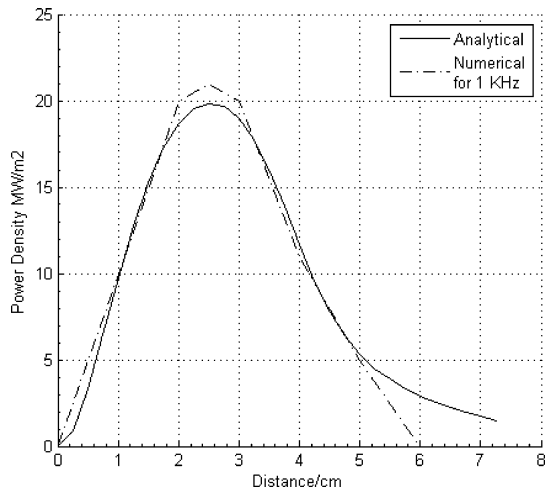

Fig. 8. Power density distribution with distance for single-coil induction heating system.

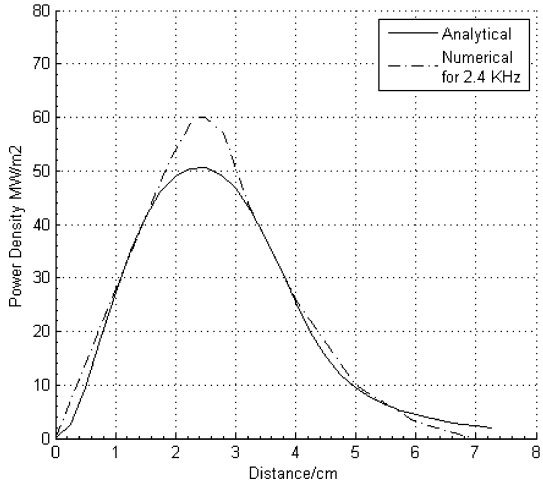

Fig. 9. Power density distribution with distance for single-coil induction heating system.

TABLE II
SINGLE-CONDUCTOR EXPERIMENTAL MODELS DATA

Parameter	Model 1	Model 2
Slot width S_L	0.15 m	0.007 m
Pole width P_L	5.7 m	0.456 m
Coil width W	6.0 m	0.46 m
Conductivity of steel plates	$3x10^6$moh.m^{-1}	$3x10^6$moh.m^{-1}
Relative permeability of steel plate	400	400
Steel plate dimension	1.2mX1.2m X0.012m	9.3cmX9.3cm X0.093cm
Exciting current	2190A	170A
Frequency	60 Hz	10KHz
Air gap g	0.129m	0.01m

B. Single-Conductor Excitation System

Two experimental models are presented by Earle Burkf and Lavers [6]; the first, a 60 Hz frequency excitation, and the second, a 10 KHz frequency excitation.

Table II shows the dimensions and system parameters of the 60 Hz and 10 KHz models, and their layout is shown in Fig. 10(a). The mathematical model may easily be constructed and presented as shown in Fig. 10(b).

Figs. 11 and 12 show the theoretical results obtained using the analysis presented in this paper and the experimental results presented by Earle Burkf and Lavers [6]. It can be seen that the theoretical results compare well with experimental ones.

This, of course, is to be expected since when backing iron is used, the magnetic circuit becomes better.

C. MultiCoil Excitation System

An experimental model has been constructed to predict the performance of multicoil excitation system. The core is made up of laminated electrical sheet steel, and a three-coil model has been constructed using a two-turn coil, as shown in Fig. 13(a). Table III shows the dimensions and system parameters of the experimental model.

The multilayer mathematical model can be easily constructed, as shown in Fig. 13(b).

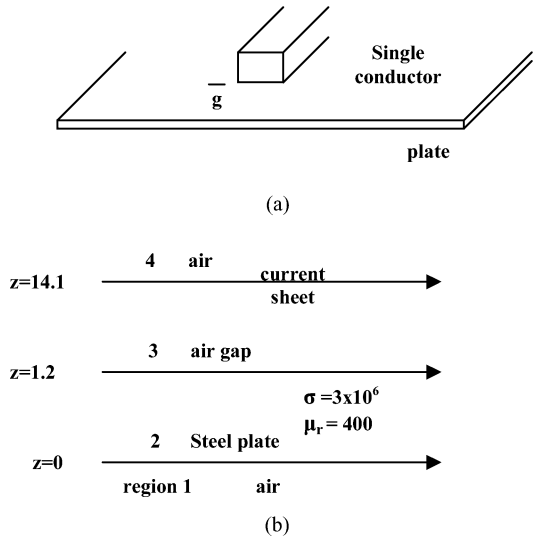

Fig. 10. Single-conductor model for 60 Hz: (a) model layout. (b) mathematical model.

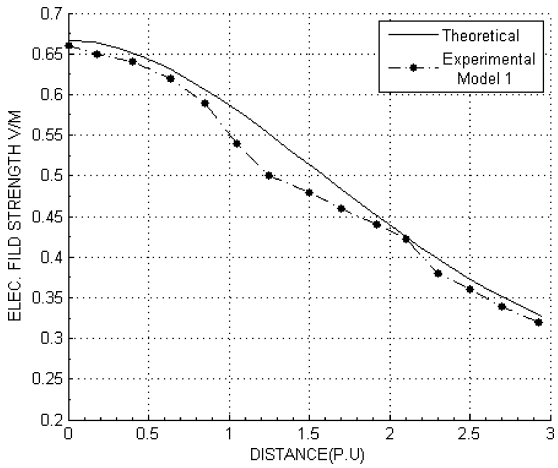

Fig. 11. Electric field distribution.

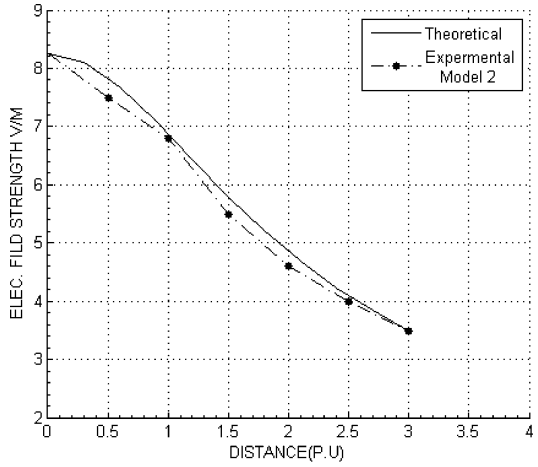

Fig. 12. Electric field distribution with distance normalized with respect to the height of bus above plate.

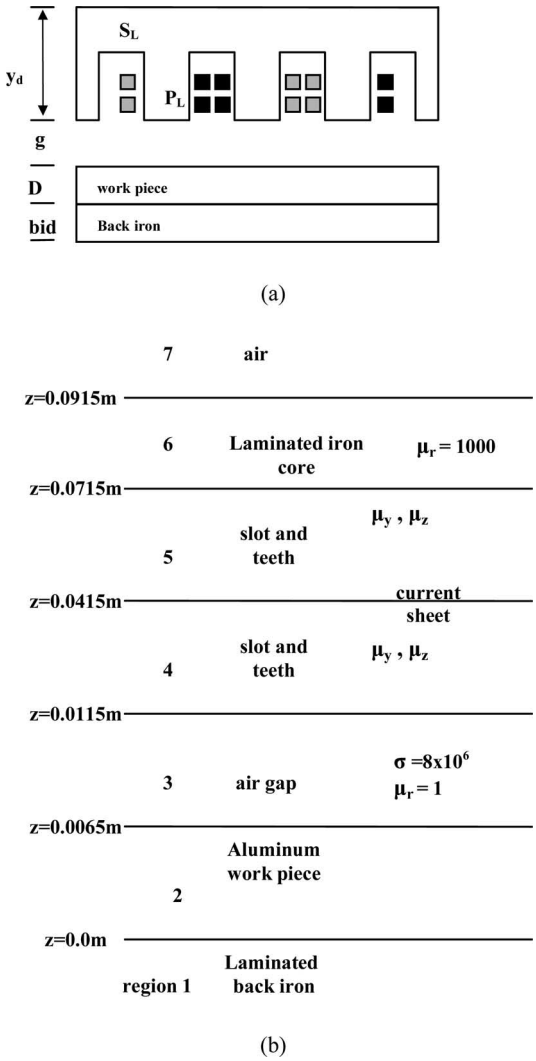

Fig. 13. Multicoil model. (a) Model layout. (b) Mathematical model.

TABLE III
MULTICOIL EXPERIMENTAL MODEL

Parameter	Value
Slot width S_L	0.02 m
Pole width P_L	0.04 m
Coil width W	0.08 m
Conductivity of Aluminum work piece	8 x 10^6 moh.m^{-1}
Work piece dimensions	0.051m X 0.32m X 0.0065m
Exciting current	300A R.M.S
Gauss meter type	F.w bell gauss/tesla meter model 4048
Air gap g	0.005 m
Work piece thickness D	0.0065 m
Yoke depth y_d	0.08 m
Back iron depth bid	0.02 m

Because of the relatively large dimensions of the slots, the current sheet is assumed to act along the central line of the slotted region bounded from both sides by an anisotropic region whose effective permeability may be calculated in the manner shown in [10].

Two tests are performed, the first with the work piece having backing iron, while the second is performed with no back iron.

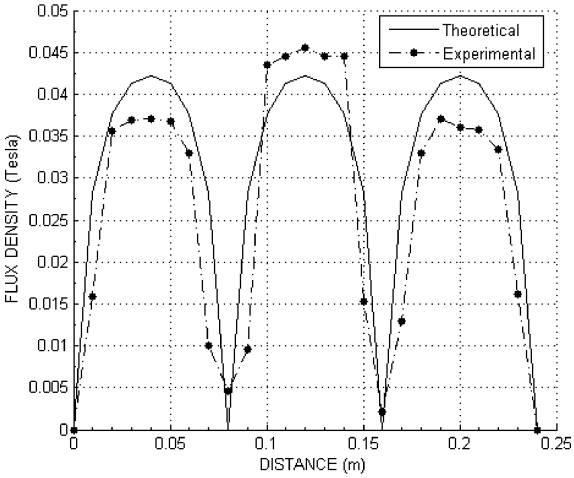

Fig. 14. Normal component of flux density with distance for single-sided induction heating system with back iron.

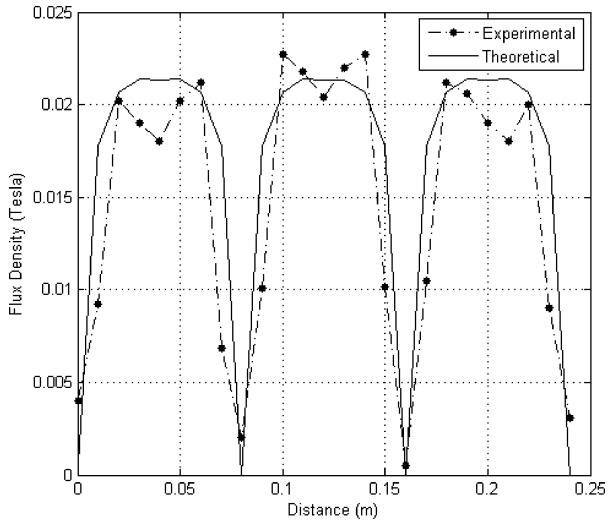

Fig. 15. Normal component of flux density with distance for single-sided induction heating system without back iron.

Figs. 14 and 15 show the results for the two tests, both experimental and theoretical.

It can be seen from the figures that considering the approximations taken in the analysis, the theoretical results correlate well with the experimental ones.

It should, however, be appreciated that for the same excitation, the flux density with backing iron is more than double that obtained when no backing iron is used.

VI. Conclusion

It has been demonstrated that the method of analysis presented here is quite general and the results obtained in all cases, both experimental and those obtained from a numerical approach, compared all well with the theoretical ones obtained using the general approach.

References

[1] E. J. Davies and P. G. Simpson, *Induction Heating Hand Book*. London, U.K.: McGraw-Hill, 1979, pp. 67–95.

[2] K. Ishibashi, "Eddy current analysis of induction heating by boundary element method," *Electr. Eng. Jpn.*, vol. 104B, no. 1, pp. 149–156, 1984.

[3] A. Patecki and G. Szymanki, "Active power loss in thick plate generated by one side inductor heater," *IEEE Trans. Magn.*, vol. MAG-17, no. 6, pp. 3271–3273, Nov. 1981.

[4] K. V. Namjoshi and P. P. Biringer, "Surface power distribution in cross fields heating of thin non magnetic plates," *IEEE Trans. Magn.*, vol. 28, no. 5, pp. 2238–2240, Sep. 1992.

[5] S. K. Sultan, "Surface induction heating," M.Sc. thesis, Univ. Baghdad, Basra, Iraq, 1997.

[6] P. Earle Burke and J. D. Lavers, "The use of modeling methods in the design of electro heat equipment," *IEEE Trans. Ind. Appl.*, vol. IA-19, no. 1, pp. 57–63, Jan./Feb. 1983.

[7] L. Gong, R. Hagel, K. Zhang, and R. Unbehaue, "On the 3-D eddy current field coupled to the heat transfer of induction heating of a slab," in *IEEE Ind. Appl. Conf. Rec.*, 1995, vol. 3, pp. 1952–1956.

[8] J. Accro, R. Alonso, J. M. Burdio, L. A. Barragan, and D. Puyal, "Analytical equivalent impedance for a planar circular induction heating system," *IEEE Trans. Magn.*, vol. 42, no. 1, pp. 84–86, Jan. 2006.

[9] J. Greig and E. M. Freeman, "Travelling wave problem in electric machines," *Proc. Inst. Electr. Eng.*, vol. 114, no. 11, pp. 1681–1683, Nov. 1967.

[10] E. M. Freeman, "Travelling waves in induction machines: Input impedance and equivalent circuits," *Proc. Inst. Electr. Eng.*, vol. 115, no. 12, pp. 1772–1776, Dec. 1968.

J. H. H. Alwash (M'02) was born in Babylon, Iraq, on March 7, 1945. He graduated from University College London, London, U.K., in 1967 and received the Ph.D degree from London University, London, in 1972 as an internal student of both Kings College, London, and Imperial College of Science and Technology, London.

He is currently a Professor in the Electrical Engineering Department, University of Baghdad, Baghdad, Iraq. His current research interests include induction machines (rotary, flat, linear, and tubular linear types) and induction heating.

S. K. Sultan was born in Baghdad, Iraq, on September 7, 1962. He received the B.Sc. degree in electrical engineering and the M.Sc. degree in power and electrical machines from the College of Engineering, University of Baghdad, Baghdad, in 1984 and 1997, respectively.

He is currently with the Electrical Engineering Department, College of Engineering, University of Baghdad, Baghdad, Iraq.